UNIVERSIDAD DISTRITAL
FRANCISCO JOSÉ DE CALDAS

Research

Study Of the Effect of Titanium Additions on The Mechanical and Corrosion Properties of AISI 316 Powder Metallurgical Steel

Estudio del efecto de adiciones de titanio en las propiedades mecánicas y de corrosión del acero pulvimetalúrgico AISI 316

Luz Adriana Cañas Mendoza[1] 🔗✉*, Yaneth Pineda Triana[2] 🔗, and Lais Mujica Roncery[2] 🔗

[1]Universidad Tecnológica de Pereira (Pereira, Colombia)-Universidad Pedagógica y Tecnológica de Colombia (Tunja, Colombia)
[2]Universidad Pedagógica y Tecnológica de Colombia (Tunja, Colombia)

Abstract

Context: Powder metallurgy uses metallic and/or non-metallic powders that, through mixing, compacting, and sintering operations, allow obtaining large series of products. In austenitic stainless steels, $Cr_{23}C_6$-type carbides can precipitate at temperatures between 450 and 950 °C. When this occurs, the steel is susceptible to being attacked at its grain boundaries by a phenomenon called *sensitization*. Titanium is added as a 'stabilizer' because it has a greater affinity with carbon for the formation of species at a temperature of approximately 900 ºC, and, during cooling it consumes the carbon forming MC-type carbides, inhibiting the precipitation of $Cr_{23}C_6$.

Method: The composition and morphology of the powders were characterized, leading to the formulation of an alloy matrix consisting of a mixture of AISI 316 steel powders of two different particle-size distributions in a proportion that produced the highest density and the lowest porosity in the sintered material. Titanium was added at two levels (0,4 and 1,0 wt %), and sintering was carried out with nitrogen. The corrosion rate was determined by potentiodynamic polarization. Vickers hardness and pin-on-disk wear tests were performed. The stages were complemented with a microstructural analysis.

Results: The addition of 0,4 wt % of titanium decreased the steel's rate of corrosion, albeit in the absence of passivation. The microstructure consists of austenite, ferrite, and TiC precipitates. The addition of 1,0 wt %Ti showed an increase in the corrosion rate, with a microstructure containing austenite, ferrite, TiC carbides, and the Laves η-Fe_2Ti phase.

Conclusions: The results were compared against thermodynamic simulations in the Thermo-Calc software, which were consistent with the microstructural analysis, showing the phenomena of stabilization as well as the precipitation of intermetallic phases and highlighting the importance of establishing strict controls in the formulation of powder metallurgical alloys due to the transformations that can take place due to the effect of the thermal cycles of the process.

Keywords: powder metallurgy, sensitization, stabilization, sintering, austenitic stainless steels

*✉ **Correspondence:** luzadriana@utp.edu.co

Resumen

Contexto: La pulvimetalurgia utiliza polvos metálicos y/o no metálicos que, mediante operaciones de mezcla, compactación y sinterización, permiten obtener grandes series de productos. En los aceros inoxidables austeníticos, los carburos de tipo $Cr_{23}C_6$ pueden precipitar a temperaturas entre 450 y 950 °C. Cuando esto ocurre, el acero es susceptible de ser atacado en sus límites de grano por el fenómeno denominado *sensitización*. El titanio se agrega como 'estabilizador' porque tiene mayor afinidad con el carbono para la formación de especies a una temperatura de aproximadamente 900 ºC y, durante el enfriamiento, consume el carbono formando carburos tipo MC, inhibiendo la precipitación de $Cr_{23}C_6$.

Método: Se caracterizó la composición y morfología de los polvos, lo que condujo a la formulación de una matriz de aleación compuesta por una mezcla de polvos de acero AISI 316 de dos granulometrías diferentes en una proporción que produjo la mayor densidad y la menor porosidad del material sinterizado. Se añadió titanio en dos niveles (0,4 y 1,0 % en peso) y se sinterizó con nitrógeno. La velocidad de corrosión se determinó por polarización potenciodinámica. Se realizaron pruebas de dureza Vickers y de desgaste *pin-on-disk*. Las etapas se complementaron con un análisis microestructural.

Resultados: La adición de 0,4 % en peso de titanio disminuyó la velocidad de corrosión del acero, si bien en ausencia de pasivación. La microestructura consiste en precipitados de austenita, ferrita y TiC. La adición de 1,0 % en peso de Ti mostró un aumento en la velocidad de corrosión, con una microestructura que contenía austenita, ferrita, carburos de TiC y la fase Laves η-Fe_2Ti.

Conclusiones: Los resultados fueron comparados con simulaciones termodinámicas del *software* Thermo-Calc, consistentes con el análisis microestructural, mostrando los fenómenos de estabilización y la precipitación de fases intermetálicas, y destacando la importancia de establecer un control estricto en la formulación de aleaciones pulvimetalúrgicas debido a las transformaciones que pueden generarse por efecto de los ciclos térmicos del proceso.

Palabras clave: pulvimetalurgia, sensitización, estabilización, sinterización, aceros inoxidables austeníticos

Table of contents

1. Introduction

In the worldwide metallic materials manufacturing industry, powder metallurgy has been progressively gaining prominence. This is due to the versatility of the process and the feasibility of manufacturing parts using different types of matrices, allowing for a wide variety of morphologies, in addition to the possibility of using different compaction, sintering, and finishing treatment processes to obtain parts with special properties (1). The industrial applications of powder metallurgical stainless

steels have increased, although they continue to represent a small fraction with respect to their forged counterparts, especially in terms of behavior against corrosion. Most stainless- steel and other high-alloy powders are made by spraying into water or by inert gas and centrifugal spraying. Water-atomized powders have an irregular particle shape and are widely used for cold compaction and sintering. The densities of sintered parts are typically below 95 % of their theoretical values, which is why their mechanical and physical properties are unfavorable compared to those of dense materials. The corrosion behavior of powder metallurgical stainless steels depends on the synergistic effect of factors such as the chemical composition (which determines the quality of the passive layer and the efficiency of the protection against the environment), the surface conditions of the component, the intermetallic phases that are unfavorable for corrosion resistance, interconnected pores (because they increase the exposed surface area), and the amount, morphology, and size of the pores (2).

Compaction and densification are difficult tasks during the sintering of stainless-steel powders due to their strength, hardness, and work hardening. Depending on the particle size distribution, compaction pressure, and sintering temperature, the sintering density is normally between 80 and 90 % of the theoretical value. The low final density and interconnected porosity cause poor mechanical properties and low corrosion resistance (3, 4) observed that the porosity of powder metallurgical products manufactured by the conventional route affects their mechanical properties at room temperature, that the behavior under fatigue conditions improves when the porosities are fine and rounded, and that this behavior worsens when there are coarse and angular porosities. This is because the pores contribute to the initiation and propagation of cracks under fatigue conditions. Other factors affect the behavior of these materials under dynamic stresses. For instance, the fatigue behavior of PM austenitic stainless steels is also affected by precipitates (carbides, nitrides) and the microstructure of the matrix. The study by (5) analyzed the effect of porosity on the microstructure and mechanical properties of 316L powder metallurgical steel for use in implants. It was found that tensile and fatigue strength increased in samples sintered with higher density. Components with low density and larger, irregular, and clustered pores showed higher deformation and premature failure.

Austenitic stainless steels have higher corrosion resistance than ferritic and martensitic stainless steels, but they are susceptible to sensitization. This phenomenon consists of a loss of corrosion resistance when steels are slowly cooled from the dissolution temperature (1.100 °C) or when they are heated to temperatures between 500 and 850 °C. When an austenitic steel containing more than 0,03 % carbon is heated above 500 °C, chromium carbides begin to form at the junctions of the austenite grains. These carbides have a variable composition, their chromium content is between 30 and 90 %, and their carbon content is between 1 and 2 %. The carbides are formed from the carbon and chromium of the nearest austenite crystals. The crystals are poorer in these elements due to the decrease in the percentages of chromium and carbon in said areas. The steel located in the vicinity of the carbides ceases to be stainless (%Cr less than 11 %), and it is attacked by chemical agents (6). This phenomenon is common in processes that are carried out at temperatures around the critical range, as is the case of welding or cooling after sintering in powder metallurgy. A method to counteract the sensitization that generates localized corrosion in grain boundaries or intergranular corrosion (CIG) consists of thermally treating redissolution of carbides. This involves heating the component to temperatures

between 1.050 and 1.150 °C. The goal is for the alloying elements to be in a solid solution, followed by rapid cooling to room temperature to prevent the formation of new carbides (7). Another method used to avoid sensitization is the addition of stabilizing elements such as titanium or niobium, as they have a greater affinity for carbon than chromium. Titanium, however, has the advantage that, once titanium carbide (TiC) forms, it does not dissolve easily in iron. When titanium-added austenitic steel is heated within the forming temperature range (700-900 °C), titanium carbides begin to precipitate instead of chromium carbides. This prevents the reduction of chromium in the austenite crystals close to the TiC. Stainless steels of this type are denoted as *stabilized*. Titanium carbides avoid sensitization since they precipitate in the austenitic matrix and improve the mechanical properties of the final part by increasing its hardness, mechanical strength, and wear resistance. Titanium additions to 316L stainless steel have also been used as biomaterials for the manufacture of implants and medical devices. In (8), it was found that the addition of boron and titanium to steel obtained via conventional powder metallurgy with nitrogen as a sintering atmosphere has a positive effect on the densification, corrosion resistance, and microhardness of the sintered components. Nitrogen diffused into the samples, producing the deposition of nitrides and favoring the formation of a superficial layer of nitrides that controlled the dissolution of the metal, thus improving resistance to corrosion in saline media.

Electrochemical methods are widely used to analyze cast and wrought stainless steels due to the quantitative information they provide about corrosion rates and mechanisms. These criteria can also be applied to sintered materials, although the presence of pores and metallurgical defects can complicate the interpretation of electrochemical data (9, 10) reduced the porosity of a powder metallurgical ferritic stainless steel by adding small gas-atomized spherical powders (AISI 316L and 430L) to larger irregular water-atomized powders (AISI 434L). The alloy obtained had the structure of duplex steel. A reduction in the number of large pores was observed, the corrosion rate decreased, and the corrosion potential increased in tests in neutral media with and without chlorides. This evaluation was carried out using electrochemical polarization tests (10).

The technological versatility of powder metallurgical processes allows varying the composition of alloys from elemental and pre-alloyed metal powders to obtain steels with improved properties. The purpose of this study was to manufacture powder metallurgical stainless steel from powders with different particle sizes and with titanium additions in order to study the changes in its physical and mechanical properties and corrosion resistance. The combination of particles with different average sizes reduced the porosity and increased the density of the preforms and sintered specimens. The addition of 0,4 wt% titanium to an AISI 316 powder metallurgical steel caused the precipitation of titanium carbides with some ferrite regions. This allowed the steel to be stabilized by preventing the precipitation of $Cr_{23}C_6$ chromium carbides. When increasing the amount of titanium to 1 wt%, the presence of the Laves η-Fe_2Ti intermetallic phase was observed nucleating from the ferrite, causing an increase in the corrosion rate of the steel. Adding titanium to the steel produced an increase in hardness and a decrease in the wear coefficient, which is explained by the precipitation of carbides and intermetallic phases. It was concluded that controlling the composition is a fundamental factor in generating microstructural changes and the precipitation of intermetallic phases, as the microstructure determines the final properties of the component.

2.   Materials and methods

The starting raw materials consisted of AISI 316 pre-alloyed stainless-steel powders with average sizes of 45 and 150 μm, elemental titanium powders of 45 μm, and zinc stearate ($Zn(C_{18}H_{35}O_2)_2$) as a lubricant in a proportion of 1 wt%. The metal powders were characterized by determining their chemical composition, size, and morphology. The tests were carried out with atomic absorption (AA) and energy dispersion spectrometry in a scanning electron microscope (SEM-EDS) for semi-quantitative elemental analysis. For the AISI 316 steel powders, the chemical composition provided by the manufacturer (GOODFELLOW) was taken as reference. The purity of the elemental titanium powders (SIGMA-ALDRICH) was confirmed via X-ray diffraction (XRD). The morphology and size of the powders were determined with a Carl Zeiss EVO MA 10 scanning electron microscope using an EHT current of 20 kV. With the secondary electron detector, the length and width of 30 different particles were measured from the acquired images. Based on this measurement, the aspect ratio (AR) was determined according to the ASTM F1877 standard (11), where AR is the ratio between the largest (d_{max}) and the smallest diameter (d_{min}). The apparent density of the metal powders was determined based on the ASTM B703 standard (12) using a cylinder of known internal volume that was filled with the sample (up to its capacity). Subsequently, the sample was weighed, and its density was determined from the ratio of mass and volume.

After characterizing the raw materials, preforms were obtained by mixing and compaction. Once the quantities of each mixture (metal powders and lubricant) were obtained, a planetary mill was used in the absence of grinding bodies for 20 minutes at 150 rpm in order to obtain a homogeneous distribution of the powders. Subsequently, uniaxial compaction was carried out, applying a pressure of 800 MPa in a universal electromechanical machine (Microtest EM/500/FR). By compacting with the established parameters, preforms with a cylindrical geometry, a diameter of 10 mm (+/- 0,15), and a height of 4 mm (+/- 0,1) were obtained.

Both the preforms and the sintered specimens were characterized by determining their density, porosity, morphology, and microstructure. The porosity was determined via image analysis with the Fiji software (ImageJ) from 30 micrographs of each specimen at a 200X magnification, which were obtained using a scanning electron microscope. The density of the preforms and the sintered samples was determined based on the procedure described by the ASTM B962 standard (13): via a gravimetric technique using deionized water and impregnation oil.

Sample sintering was performed in a CARBOLITE STF/TZF tube furnace using grade-four nitrogen as the sintering atmosphere and a dew point of -60 °C, which guarantees a dry and pure atmosphere (with less than 10 ppm of oxygen). The sintering temperature was set to 1.200 ºC, a value used for austenitic stainless steels (14–17). Fig. **1** shows the thermal cycles of the sintered samples.

The pre-sintering treatment carried out at 450 ºC aimed to eliminate the lubricant and was followed by an increase in temperature to 1.200 °C for the sintering process. Afterwards, stabilization was carried out at a temperature of 900 ºC to favor the precipitation of Ti species (carbides, nitrides, and/or
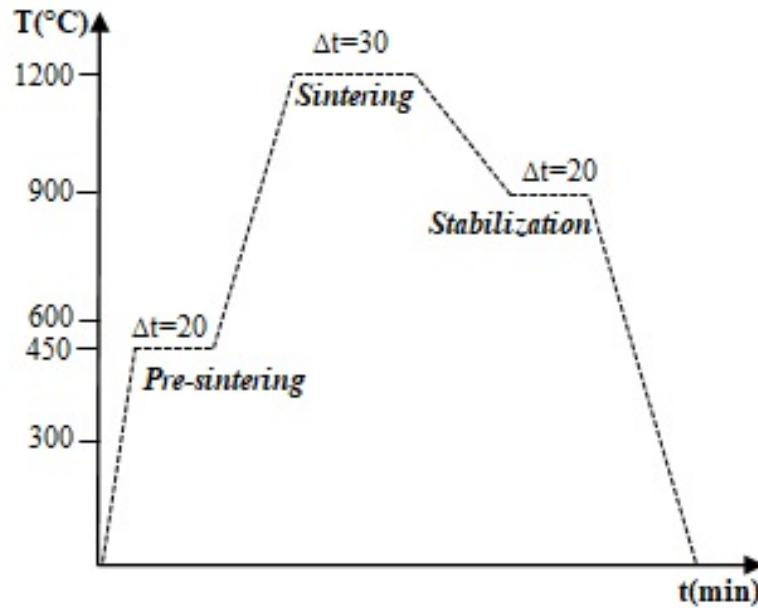
Figure 1. Thermal cycles diagram for the sintering of powder metallurgical alloys

carbonitrides), aiming to avoid chromium carbide precipitation (around 800 ℃) as well as the presence of free carbon. Quenching was performed in the water at room temperature. A characterization of the sintered samples and an evaluation of different properties were conducted to determine the effects of modifying the composition of AISI 316 powder metallurgical steel by adding titanium as an alloying element.

Mechanical properties such as hardness were determined under the guidelines of the ASTM E384 standard for measurement on the Vickers HV scale [18]. A QV-1000DM Micro Vickers Hardness Tester was used, applying a load of 100 gf for 20 seconds. A wear resistance evaluation was carried out via the pin-on-disk test, according to the ASTM G99 standard [19], using a MT/60/NI Microtest tribometer.

Corrosion resistance was evaluated through electrochemical tests, obtaining potentiodynamic polarization curves while using a GAMRY 750 Potentiostat Galvanostat at room temperature. The linear polarization resistance (LPR) and the active/passive characteristics of the metal/solution system were determined, and the corrosion rate (in mpy) was calculated. The samples were polished on 2000 sandpaper as surface preparation before testing. Each sample was placed in a cell with a hole of a known area, using a 1N H_2SO_4 solution with 250 ppm NaCl as the electrolyte. An Ag/AgCl (3M KCl) reference electrode and a platinum counter electrode were used. A first test was carried out to determine the open circuit potential. The LPR was determined by employing a potential difference of ±20 mV concerning this value. Potentiodynamic polarization tests were performed with a potential difference of -400 mV for the cathodic polarization and with +1500 mV for the anodic curve. This, in order to determine the passivation and transpassivation zones. The tests were carried out while taking the ASTM G3, ASTM G5, ASTM G59, and ASTM G102 standards as reference [20–23].

3. Results and discussion

The results obtained during the characterization of the metallic powders, the preforms, and the sintered samples are presented below. Fig. 2 shows the micrographs, obtained via scanning electron microscopy (SEM); the chemical composition, determined by energy dispersion spectrometry (EDS) and atomic absorption (AA) in comparison with the values provided by the powder suppliers; and the diffractograms, obtained using X-ray diffraction (XRD) on the metallic powders.
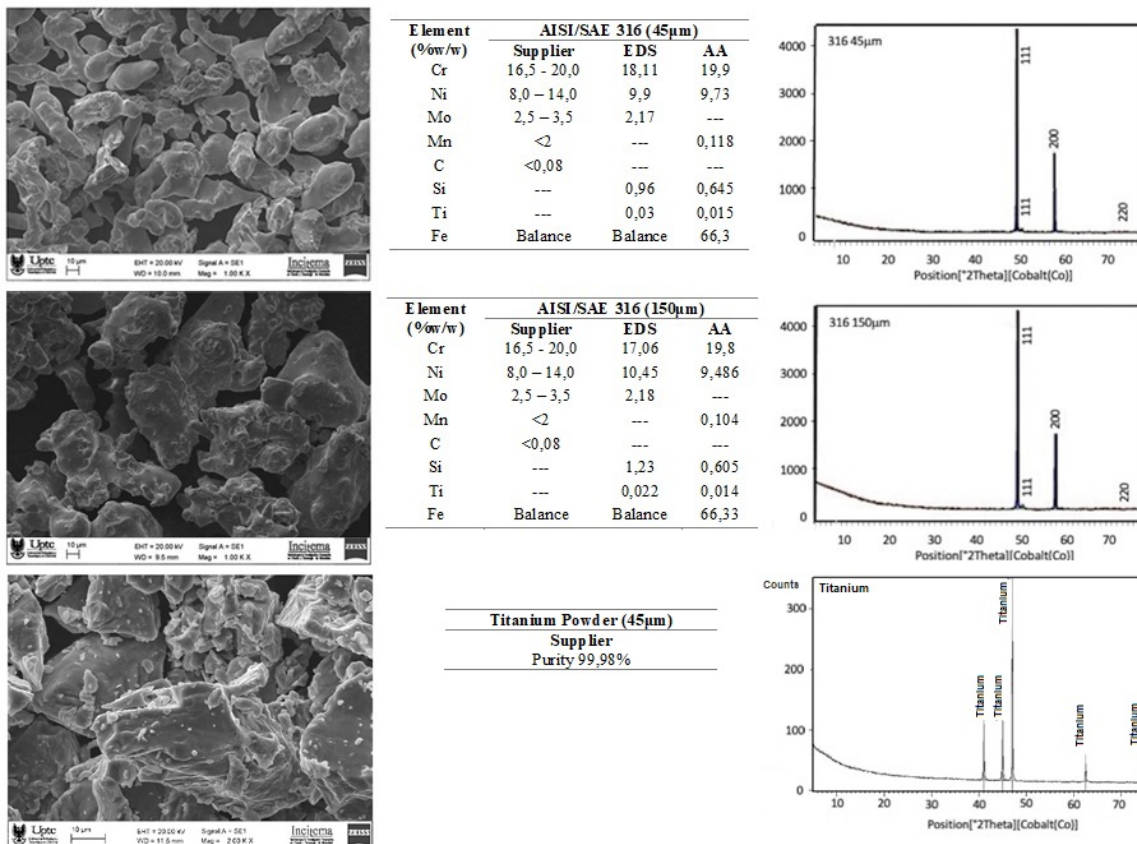
Figure 2. SEM micrographs, chemical composition (EDS, AA), and diffractograms (XRD) of metallic powders

The values obtained through the characterization techniques confirm that the elements are within the range provided by the supplier. For the two types of AISI 316 steel powders, diffraction planes (111), (200), and (220) are observed, corresponding to the face-centered cubic structure of austenite. The diffractograms confirm the purity of the elemental titanium powders. Fig. 2 shows that, for the AISI 316 steel powders, the particles have an irregular shape, typical of the water atomization process; whereas, for the titanium powders, the morphology is sponge-like, as these stem from grinding a sponge made (*i.e.*, the Kroll process), resulting in irregular particles. In both cases, the morphologies are appropriate for alloy compaction and sintering processes. The Aspect Ratio (AR) for the 45 μm AISI 316 powders was 1,4406, and, for the 150 µm powders, it was 1,5692. These AR values confirm the irregular shape of the particles. Table I shows the apparent density values of the metal powders.

Table I. Apparent density of metallic powders

Apparent density of 316 steel powders (45 μm)	Apparent density of 316 steel powders (150 μm)	Apparent density of titanium powders (45 μm)
3,1566 g/cm^3	3,2148 g/cm^3	2,0923 g/cm^3

The low apparent density values are related to unsettled particles and voids. Because a volume greater than the real one is taken, the calculated density is lower than the actual value (hence the term *apparent*).

In preliminary tests, five types of mixtures of 45 and 150 μm AISI 316 steel powders were evaluated in order to define the most appropriate mixture in terms of the highest density, the lowest porosity, and the lowest corrosion rate. Based on these results, the alloy matrix was defined, which consists of a mixture of 65 wt% of 150 μm AISI 316 powders and 35 wt% of 45 μm AISI 316 powders. With this matrix, the alloys with titanium additions were prepared. Based on the composition of stabilized austenitic stainless steels (AISI 321), where the recommended amount of titanium is about five times the percentage of carbon, which exceeds 0,02 wt%, and considering the nitrogen traces, additions of 0,4 and 1,0 wt%Ti were established. With these percentages, we expected to have enough titanium to stabilize the alloy, as well as an additional amount aiming at the formation of other species such as carbides, nitrides, and/or carbonitrides. Table **II** presents the nomenclature of the samples and the properties determined for both the preforms and the sintered samples.

Table II. Sample characterization results

Sample	Porosity (%)		Density (g/cm^3)		Hardness (HV)	Wear coefficient (mm^3/N.mm)	Wear depth (μm)
	Preforms	Sintered	Preforms	Sintered			
1(316)	5,90	4,69	7,12	7,66	231	1,18E-06	48,6
2(316+0,4Ti)	5,82	4,43	7,14	7,67	255	2,51E-07	24,7
3(316+1Ti)	5,56	4,36	7,21	7,70	251	2,59E-07	21,0

Table **II** shows the variations in the porosity and density of the preforms and sintered samples, where the effect of the sintering process is observed in the elimination of part of the interconnected porosities between the powder particles, given that all the porosity values of the sintered samples are below their green counterparts. It is also evident that the addition of titanium generates lower porosity values and higher densities for the evaluated ranges and the two types of samples (preforms and sintered samples).

This behavior is due to the size of the particles, as the matrix combines 150 and 45 μm AISI 316 steel powders and the average size of the titanium powders is 45 μm. Therefore, in Fig. **3**, it is observed that the titanium is arranged in the spaces formed between the largest particles, favoring the reduction of empty spaces and increasing packing.
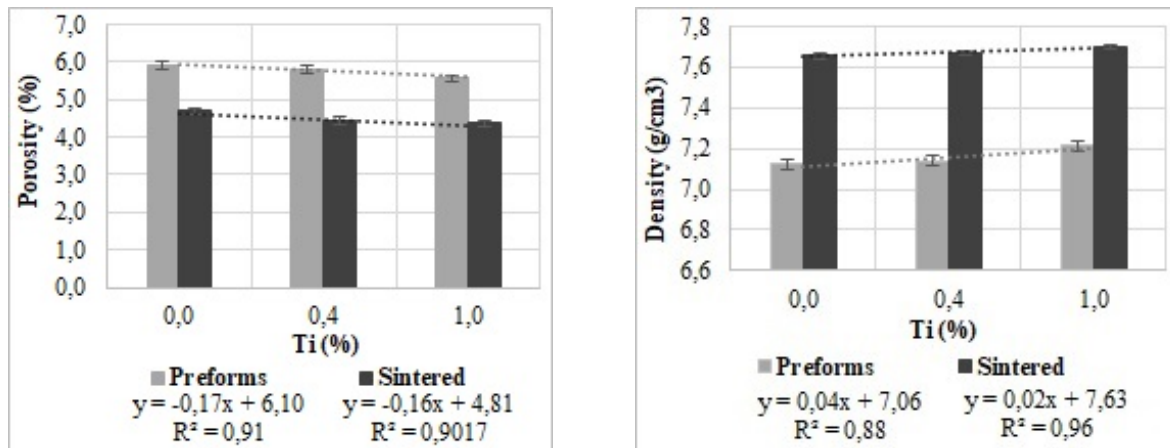
Figure 3. Morphology of preforms determined by SEM (EHT=20,00KV, SIGNAL A=SE1, WD=11 mm, MAG= 70 x 100 μm)

Regarding the results obtained for hardness (Table 2), the alloys containing titanium have increased hardness when compared to Ti-free steel. In the case of the wear coefficient and the wear depth generated during the pin-on-disk test, the addition of 0,4 wt%Ti causes a drastic decrease in the two properties, with minimal variations when adding 1,0 wt% of the alloy element.

The effect of adding titanium on the mechanical and tribological properties of AISI 316 steel is supported by the microstructural observation presented after the corrosion resistance results. Table **III** shows the results obtained in the potentiodynamic tests aimed at determining the corrosion rate of the alloys.

Table III. Results obtained via potentiodynamic tests for sintered alloys. Electrolyte: 1N H_2SO_4 solution with 250ppm NaCl; reference electrode (Ag/AgCl 3M KCl); platinum counter electrode

Sample	β_a [mV/decade]	β_c [mV/decade]	i_{corr} [mA/cm^2]	E_{corr} [mV]	LPR [Ohms]	Vcorr [mpy]
1(316)	7,07	7,58	0,00238	-518,4	854,9	**1,07**
2(316+0,4Ti)	699,70	449,80	0,00168	-553,6	90.490,0	**0,76**
3(316+1Ti)	3,82	3,41	0,00231	-586,6	434,2	**1,04**

The results show that the addition of 0,4 wt%Ti reduces the corrosion rate of the sintered steel to the minimum value obtained, and it is observed that higher additions have an adverse effect, as the corrosion rate increases from 0,76 mpy in sample 2(316+0,4Ti) to 1,04 mpy in sample 3(316+1Ti), which corresponds to a growth of 1,4 orders of magnitude, with the latter value approaching that reported for steel without titanium. The analysis of the behavior of the materials under study requires observing the graphs obtained in the polarization tests, which represent the variables necessary to determine the rate of corrosion, as well as the active/passive behavior of the samples' surface. Fig. 4 shows the measured polarization curves of the sintered samples.
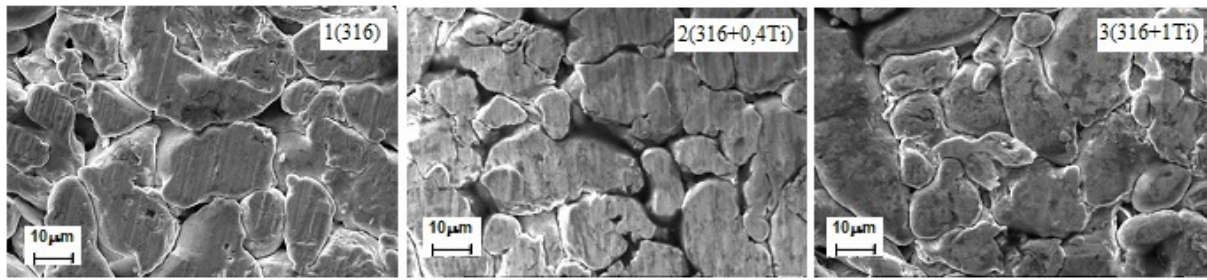
Figure 4. Tafel curves of potentiodynamic polarization for the sintered steels. Electrolyte: 1N H2SO4, 250 ppm NaCl

According to Fig. **4**, the behavior is similar for samples 1(316) and 3(316+1Ti), in which the formation of the passive film is observed in the intermediate range between the passivation and transpassivation potentials. Although the corrosion rates calculated for these samples from the Tafel slopes and the linear polarization resistance LPR are very close, the sample with 1 wt %Ti shows a higher and unstable passivation current ip. Both curves show that the current tends to increase in the passivation range. On the other hand, sample 2(316+0,4Ti) does not show a critical passivation current but a lower and more stable current which could be associated with the formation of a passive layer. The addition of 0,4 wt %Ti shifts the corrosion and passivation currents towards lower values with regard to the other samples, which produces a lower corrosion rate. The potentiodynamic graphs of this composition show that the steel passed directly to the passivation zone without going through the dissolution zone.

Based on the chemical composition of each alloy, the Thermo-Calc software was used to predict the equilibrium phases via computational thermodynamics. Calculations were carried out at the sinterization and stabilization temperatures described in Fig. **1**. The compositions used in the software correspond to those determined during the experimental characterization of metal powders, with the aim of obtaining results consistent with the material. Phase quantification was performed for each alloy during these two stages, highlighting that the final microstructure corresponds to the one formed during the stabilization stage (900 °C). Table **IV** shows the theoretical percentages of the phases present.

Table IV. Quantification (molar fraction) of phases in sintered alloys (sinterization + stabilization) in Thermo-Calc

Sample/Phases	Austenite (γ)	Ferrite (α)	$Cr_{23}C_6$	Ti(C,N)	Laves (η)	TOTAL
1(316)	0,99		0,01			1
2(316+0,4Ti)	0,97	0,02		0,01		1
3(316+1Ti)	0,85	0,13		0,01	0,01	1

Because the interaction of the elements generates the precipitation of different phases, the aforementioned simulation tool allows analyzing the microstructural observation. Thus, according to the theoretical calculations, the presence of chromium carbides ($Cr_{23}C_6$), titanium compounds with

carbon and/or nitrogen Ti(C,N), and probably an intermetallic Laves(η) phase is expected. Fig. **5** shows the observed microstructures.
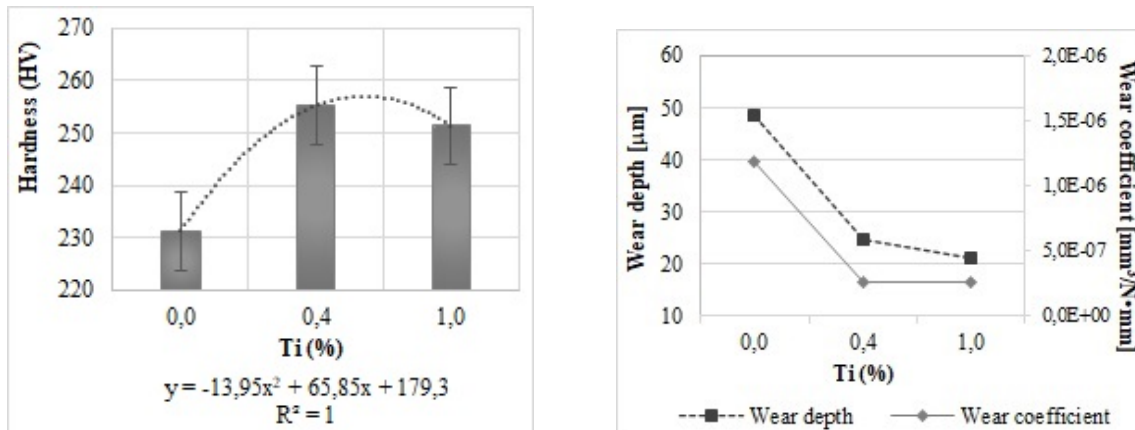
Figure 5. Micrographs of sintered alloys. a) Sample 1(316) obtained via SEM, b) sample 2(316+0.4Ti) obtained via SEM, 3) sample 3(316+1Ti) obtained via OM (left) and SEM (right)

Fig. **5**a shows the micrograph of sample 1(316) obtained via SEM with backscattered electrons. The observation was complemented with elemental mapping, showing the presence of carbon in grain boundaries, which is attributed to the formation of carbides. The remaining porosity in the sintered alloy offers favorable sites for the deposition of oxides, which, in this case, may correspond to those formed from the silicon detected in the characterization. Open and unconnected porosities remain, with a rounded and elongated morphology. Carbides of the $Cr_{23}C_6$ form preferentially precipitate at the grain boundaries on the surface of the pores, although there are small depositions of these carbides inside the grains. There is agreement with the structure projected with the thermodynamic calculations, although, qualitatively, the percentage of carbides seems to exceed the value predicted by the software.

The microstructure observed in Fig. **5**b, obtained via SEM with backscattered electrons for sample 2(316+0,4Ti), is distributed as determined by the software, since it consists of austenite grains with intragranular precipitates of TiC (nitrides, which have an elongated morphology, were not identified in these samples). Ferrite regions (α) were also observed in the areas of high pore density. No intermetallic phase or $Cr_{23}C_6$ chromium carbide precipitates were found. With this composition, titanium meets the objective of stabilization, avoiding the sensitization of stainless steel.

Fig. **5**c shows micrographs (OM and SEM) of sample 3(316+1Ti), in which the theoretically predicted phases can be identified. The high titanium content has two main effects on the microstructure: it inhibits the precipitation of chromium carbides ($Cr_{23}C_6$) and, in turn, induces the presence of the Laves η-Fe_2Ti phase. The precipitation of intermetallic phases is counterproductive to the stabilization of the material. The microstructures show the deposition of intragranular titanium carbides and nitrides. According to the observed distribution, it can be inferred that the Laves η-Fe_2Ti phase nucleates from the interior of the ferrite (α), taking advantage of the titanium from this solid solution. Apparently, there are some regions where this intermetallic phase has grown to consume the ferrite. In addition to the phase distribution, it is observed that, in general, the remaining porosity of the material is located in the

ferrite regions (α). The elemental distribution of titanium observed by SEM suggests that its diffusion begins at the surface of the Fe(α) particles, initially stabilizing the Fe(α) phase, up to a saturation point that produces a concentration gradient high enough for particle nucleation. Furthermore, the laminar topology of the intermetallic compound η-Fe$_2$Ti confirms its precipitation by diffusion inside the ferrite. For these samples, it can be concluded that, although the observed phases coincide with the predicted ones, the observed amounts differ from the theoretical ones, *i.e.*, a higher percentage of the Laves phase η-Fe$_2$Ti and a lower percentage of Fe(α) in comparison with the calculated values (Table IV). The Laves phase (η) is the name given to intermetallic compounds with a hexagonal-type unitary cell, whose shape depends on the composition of the alloy, which can vary between Fe$_2$Mo and Fe$_2$Ti.

The contrast of the microstructures observed in the three alloys explains the results regarding their performance. The increase in hardness and the decrease in the wear coefficient due to the presence of titanium when compared to the first sample is attributed to the precipitation of TiC carbides that are deposited inside the grains. These carbides are present as secondary phases, and their formation takes advantage of carbon in a solid solution. As for the corrosion rate, alloy 1(316) shows the presence of chromium carbides (Cr$_{23}$C$_6$), which cause the sensitization of austenitic stainless steels, generating a high rate of corrosion, since, as per its stoichiometry, it is a Chromium-rich compound that precipitates at the grain boundaries of austenite. In case of alloy 2(316+0,4Ti), the stabilization of the steel was achieved, avoiding the phenomenon of sensitization. Therefore, this alloy exhibits the lowest corrosion rates. In the 3(316+1Ti) alloy, the presence of ferrite and the intermetallic compound Laves η-Fe$_2$Ti was observed, with the formation of a passive layer, which is expected for this type of steel. It was observed that, if the titanium content is higher than that required for stabilization, it generates a detriment in the corrosion rate (24, 25).

4.   Conclusions

Titanium additions in AISI 316 powder metallurgical stainless steel decrease the porosity and increase the density of the preforms, and therefore of the sintered samples. This proves the importance of combining particles of different sizes to obtain less porous components and higher densification in manufacturing processes through conventional powder metallurgy.

The direct relationship between the wear depth generated with the pin-on-disk test and the wear coefficient was confirmed. By determining the mechanical properties of the alloys studied, it was observed that the hardness of a powder metallurgical steel made from AISI 316 significantly increases when titanium is incorporated due to the precipitation of titanium compounds, *i.e.*, Ti(C,N).

The performance reported in the potentiodynamic polarization tests, complemented with a microstructural analysis, showed that the addition of 0,4 wt %Ti to AISI 316 powder metallurgical steel decreases its corrosion rate by preventing the precipitation of intermetallic compounds and Cr$_{23}$C$_6$ chromium carbides. In this case, titanium performs its function in the stabilization of the steel, avoiding sensitization. With larger additions of the alloying element, an adverse effect was observed, due to the precipitation of the Laves η-Fe$_2$Ti phase.

Changes in the composition of systems as complex as stainless steels, which are made by increasing the proportion of their alloying elements, do not guarantee improved properties in terms of corrosion resistance, since a series of phenomena come into play which involve atomic diffusion processes, thermodynamic energy favorable for the formation of certain compounds, and concentration gradients when the modified elements do not dissolve within the ferrous matrix. Added to the above, the morphology of steels obtained through manufacturing processes using conventional powder metallurgical methods makes it impossible to eliminate porosity in the final product.

The modification of the initial composition of AISI 316 austenitic stainless steel allows concluding that the addition of 0,4 wt % of elemental titanium improves its mechanical properties, reduces the rate of electrochemical corrosion of the alloy, promoting the precipitation of titanium carbides, and achieves stabilization. The potentiodynamic plots of this composition show that the steel changed directly to the passivation zone without going through the dissolution zone.

5. Acknowledgements

6. CRediT author statement

Luz Adriana Cañas: Conceptualization, investigation, methodology, formal analysis, visualization, writing: original draft.
Yaneth Pineda Triana: Formal analysis, funding acquisition, project administration, resources, supervision, visualization, writing: review and editing.
Lais Mujica Roncery: Formal analysis, visualization, writing: review and editing.

References

[1] M. Groover, *Fundamentos de manufactura moderna: materiales, procesos y sistemas*, 3rd ed., New York, NY, USA: McGraw-Hill, 2007. ↑2

[2] A. Szewczyk-Nykiel, "The influence of molybdenum on corrosion resistance of sintered austenitic stainless steels," *Tech. Trans.*, vol. 2015, pp. 131-142, 2015. https://doi.org/10.4467/2353737XCT.15.344.4865 ↑3

[3] M. Rosso, "Contribution to study and development of PM stainless steels with improved properties," *J. Achievements Mater. Manuf. Eng.*, vol. 24, no. 1, p. 178, 2017. https:

//www.researchgate.net/publication/40804796_Contribution_to_study_and_
development_of_PM_stainless_steels_with_improved_properties ↑3

[4] S. Schmid and S. Kalpakjian, *Manufactura, ingeniería y tecnología*, 5 ed., México: Pearson-Prentice Hall, 2008. ↑3

[5] N. Kurgan, Effect of porosity and density on the mechanical and microstructural properties of sintered 316L stainless steel implant materials," *Mater. Design*, vol. 55, p. 235-241, 2014. https://doi.org/10.1016/j.matdes.2013.09.058 ↑3

[6] J. J. Ibáñez Montenegro, "Estudio de la soldadura en aceros austeníticos," undergraduate thesis, Fac. Ingeniería, Univ. Piura, Carabobo, Venezuela, 2005. ↑3

[7] J. P. Vázquez, "Estudio de la precipitación de carburos en el acero inoxidable AISI 304 en enfriamiento continuo," Master's thesis, Fac. Ing. Mec. Elec., Univ. Autónoma de Nuevo León, Nuevo León, México, 1996. ↑4

[8] S. Ali *et al.*, "Synthesis, surface nitriding and characterization of Ti-Nb modified 316L stainless steel alloy using powder metallurgy," *Mater.*, vol. 14, no. 12, art. 3270, 2021. https://doi.org/10.3390/ma14123270 ↑4

[9] E. Klar and P. K. Samal, *Powder metallurgy stainless steels: Processing, microstructure, and properties*, Novelty, OH, USA: ASM International, 2007. ↑4

[10] Moral *et al.*, "Aqueous Corrosion Behaviour of Sintered Stainless Steels Manufactured from Mixes of Gas Atomized and Water Atomized Powders,". *Corr. Sci.*, vol. 51, no. 8. p. 1653, 2009. https://doi.org/10.1016/j.corsci.2009.04.017 ↑4

[11] *Standard Practice for Characterization of Particles*, ASTM F1877, ASTM International, 2016. https://doi.org/10.1520/F1877-16 ↑5

[12] *Standard test method for apparent density powders using Arnold meter*, ASTM B703, ASTM International, 1994. https://doi.org/10.1520/b0703-94r99e01 ↑5

[13] *Standard test methods for density of compacted or sintered powder metallurgy (PM) products using Archimedes' principle*, ASTM B962-15, ASTM International, 2015. https://doi.org/10.1520/b0962-15 ↑5

[14] G. S. Upadhyaya, *Powder metallurgy technology*, 1st ed., Cambridge, UK: Cambridge International Science Publishing, 2002. ↑5

[15] S. Ali *et al.*, "Investigation of alloy composition and sintering parameters on the corrosion resistance and microhardness of 316L stainless steel alloy," in *Advances in Manufacturing II: Lecture Notes in Mechanical Engineering*, B. Gapiński, M. Szostak, and V. Ivanov, Eds., Cham, Germany: Springer, 2019, pp. 532-541. https://doi.org/10.1007/978-3-030-16943-5_45 ↑5

[16] A.-M. Bandar, "Powder metallurgy of stainless steel: State of the art, challenges and development," in *Stainless Steel*, A. Pramanik and A. K. Basak, Eds., Jubail, Saudi Arabia: Nova Science Publishers, 2015, pp. 37-80. ↑5

[17] T. DebRoy *et al.*, "Additive manufacturing of metallic components – Process, structure and properties," *Prog. Mater. Sci.*, vol. 92, pp. 112-224, Mar. 2018. https://doi.org/10.1016/j.pmatsci.2017.10.001 ↑5

[18] *Standard test method for Knoop and Vickers hardness of materials*, ASTM E 384-11, ASTM International, 2011. https://doi.org/10.1520/e0384-10e02 ↑6

[19] *Standard test method for wear testing with a pin-on-disk apparatus*, ASTM G99-17, ASTM International, 2017. https://doi.org/10.1520/g0099-05 ↑6

[20] *Standard practice for conventions applicable to electrochemical measurements in corrosion testing*, ASTM G3-89, ASTM International, 2010. https://doi.org/10.1520/g0003 ↑6

[21] *Standard reference test method for making potentiostatic and potentiodynamic anodic polarization measurements*, ASTM G5-94, ASTM International, 2011. https://doi.org/10.1520/g0005-14e01 ↑6

[22] *Standard test method for conducting potentiodynamic polarization resistance measurements*, ASTM G59-97, ASTM International, 2020. https://doi.org/10.1520/g0059-97r14 ↑6

[23] *Standard practice for calculation of corrosion rates and related information from electrochemical measurements*, ASTM G102-89, ASTM International, 2015. https://doi.org/10.1520/g0102-89r15e01 ↑6

[24] A. F. Padilha et al., "Stainless steel heat treatment," in *Encyclopedia of Iron, Steel, and Their Alloys (Online Version)*, Taylor & Francis Group, 1st Edition, 2016, pp. 1–28. ↑12

[25] X. Q. Chen, W. Wolf, R. Podloucky, and P. Rogl, "Ab initio study of ground-state properties of the Laves phase compounds TiCr2, ZrCr2, and HfCr2," *Phys. Rev. B Condens. Matter Mater. Phys.*, vol. 71, art. 174101, 2005. https://doi.org/10.1103/PhysRevB.71.174101 ↑12

Luz Adriana Cañas Mendoza

Metallurgical engineer, Universidad Industrial de Santander (UIS), Bucaramanga, Colombia; Master of Metallurgical Engineering, Universidad Industrial de Santander (UIS), Bucaramanga, Colombia; PhD in Materials Science and Engineering, Universidad Pedagógica y Tecnológica de Colombia (UPTC), Tunja, Colombia. She is a researcher of the following research groups: Materiales Avanzados (Addvanced Materials, GIMAV), Integridad y Evaluación de Materiales (Materials Integrity and Evaluation, GIEM), and Materiales de Ingeniería (Engineering Materials, GIMI). She is a professor at Universidad Tecnológica de Pereira (UTP), Pereira, Colombia, since 2007, as well as a tutor for the Semillero de Investigación en Ingeniería y Manufactura de Materiales (Materials Engineering and Manufacturing Research Seedbed, SIIMA-UTP).
Email: luzadriana@utp.edu.co

Yaneth Pineda Triana

Metallurgical engineer, Universidad Pedagógica y Tecnológica de Colombia (UPTC), Tunja, Colombia; PhD in Mechanical and Materials Engineering, Universidad Politécnica de Valencia – Internacional; senior researcher recognized by MinCiencias (Colombian Ministry of Science, Technology, and Innovation). She is a professor at Universidad Pedagógica y Tecnológica de Colombia (UPTC), Tunja, Colombia, since 1994. Researcher and coordinator of the failure analysis area at Instituto para la Investigación y la Innovación en Ciencia y Tecnología de Materiales (Institute for Research and Innovation in Materials Science and Technology, INCITEMA); coordinator of the Master's Program in

Metallurgy and Materials Science of Universidad Pedagógica y Tecnológica de Colombia (UPTC), Tunja, Colombia; coordinator of the Doctoral Program in Materials Science and Engineering of Universidad Pedagógica y Tecnológica de Colombia (UPTC), Tunja, Colombia.
Email: yaneth.pineda@uptc.edu.co

Lais Mujica Roncery

Chemical engineer, Universidad Nacional de Colombia (UNAL), Bogotá, Colombia; Master of Chemical Engineering, Universidad Industrial de Santander (UIS), Bucaramanga, Colombia; PhD in Engineering, Ruhr- Universität Bochum, Bochum, Germany; senior researcher recognized by MinCiencias (Colombian Ministry of Science, Technology, and Innovation). She is a professor at Universidad Pedagógica y Tecnológica de Colombia (UPTC), Tunja, Colombia, since 2017. Director of Grupo de Investigación en Materiales Siderúrgicos (Siderurgic Materials Research Group) at UPTC, Tunja, Colombia (2017-2022); director of Instituto para la Investigación y la Innovación en Ciencia y Tecnología de Materiales (Institute for Research and Innovation in Materials Science and Technology, INCITEMA), Tunja, Colombia, since 2023.
Email: lais.mujica@uptc.edu.co